Liu, Qing; Meng, Zhuojun; Korpi, Antti; Kontturi, Eero; Kostiainen, Mauri A.

Cationic cellulose nanocrystals for fast, efficient and selective heparin recovery

Published in:
Chemical Engineering Journal

DOI:
10.1016/j.cej.2021.129811

Published: 15/09/2021

Document Version
Publisher's PDF, also known as Version of record

Chemical Engineering Journal 420 (2021) 129811

Contents lists available at ScienceDirect

Chemical Engineering Journal

journal homepage: www.elsevier.com/locate/cej

Cationic cellulose nanocrystals for fast, efficient and selective heparin recovery

Qing Liu [a], Zhuojun Meng [b], Antti Korpi [a], Eero Kontturi [b], Mauri A. Kostiainen [a,*]

[a] Biohybrid Materials, Department of Bioproducts and Biosystems, Aalto University, 00076 Aalto, Finland
[b] Materials Chemistry of Cellulose, Department of Bioproducts and Biosystems, Aalto University, 00076 Aalto, Finland

ARTICLE INFO

Keywords:
Heparin
Cellulose nanocrystal
Polyelectrolytes
Electrostatic interaction
Selective capture
Recyclability

ABSTRACT

Heparin is one of the most important anticoagulant agents used in clinical applications. Commercial heparin production includes an isolation from mucosa and an additional enrichment step by cationic resins. However, this process remains time-consuming while heparin is obtained in very low concentrations with the presence of macromolecular impurities, such as proteins. Therefore, an alternative with a fast, efficient and selective heparin-recovery performance is highly desirable. In this work, we utilized a biomass-derived cellulose nanocrystal colloid conjugated with cationic polyelectrolytes for heparin recovery. The high specific surface area and brush-like structure significantly increased the heparin-capture speed and efficiency under physiologically relevant conditions, which were demonstrated by the methylene blue binding assay and quartz crystal microbalance measurement. We also found that a selective heparin capture can be realized *via* adjusting salt concentration or pH. Finally, we showed that after several recycle rounds, the heparin-recovery ability of the cationic nanocrystals was largely retained and the majority of active heparin dose was recovered, showing a significantly higher heparin-recovery performance than the commercial Amberlite IRA-900 and demonstrating its applicability from an economic perspective. Therefore, the reported cellulose nanocrystal-polymer conjugate represents a promising candidate for a green and efficient heparin recovery.

1. Introduction

Heparin is a heterogeneous linear glycosaminoglycan (GAG) consisting of alternating uronic acid and D-glucosamine subunits where the primary hydroxyl and amino groups are sulfonated.[1] The existence of carboxylic and sulfonate groups makes heparin a highly charge-dense polyanion.[2] It is well-known that heparin can complex with thrombin inhibitors such as antithrombin III (ATIII) with high selectivity and affinity, and eventually inhibit blood-clotting cascade, which makes heparin one of the most effective anticoagulant agents.[2,3] Currently, heparin is the most widely used polysaccharide-based anticoagulant with an annual market of ~ 7 billion dollars in 2016.[4] The medical role of heparin has also been explored in other fields. For example, preclinical and clinical studies have suggested the antitumor ability of heparin.[5,6] Other reports have revealed that heparin can circumvent the reticuloendothelial system and selectively accumulate at tumor targets, which have attracted broad interest in drug delivery applications.[7–9]

Currently, there are several approaches in producing heparin and the extraction from porcine intestinal mucosa remains the dominant technique.[4,10] Commercial heparin production involves an initial mucosa isolation and hydrolysis step, followed by a chemical digestion or autolysis, yielding partially purified heparin in very low concentrations (~0.01 wt%).[10] As a result, a heparin-enrichment step is commonly needed before further purification. Heparin possesses the highest charge density among all known biomacromolecules (~3.7 negative charges/disaccharide) and is the most strongly interacting target through electrostatic interaction.[11,12] Therefore, plenty of synthetic polycations or engineered proteins have been prepared to bind heparin.[13–15] Quaternized ammonium cations that are either immobilized on resins or able to precipitate heparin are prevalent for heparin binding and recovery.[10] Currently, a number of quaternized ammonium cation functionalized resins are commercially available for this purpose, such as Amberlite-IRA900 and Dowex 22CL, and they are feasible for recycling.[10] Nevertheless, continuous efforts are dedicated to the discovery of novel alternatives, attempting to improve the heparin-recovery efficiency.[16–18] More importantly, commercial resins are derived from petroleum-based synthetic beads.[10] Mounting evidence has

* Corresponding author.
E-mail address: mauri.kostiainen@aalto.fi (M.A. Kostiainen).

https://doi.org/10.1016/j.cej.2021.129811
Received 8 March 2021; Received in revised form 1 April 2021; Accepted 9 April 2021
Available online 15 April 2021

unveiled that plastic products can be eventually fragmented into small microplastics which present hazard to various organisms throughout the ecosystem.[19,20] Therefore, environment-friendly alternatives with an excellent heparin-recovery performance are highly desirable. Chitosan, the naturally derived product from chitin, has been proposed to fulfill the task as chitin is a highly abundant biopolymer and the presence of amino groups enables binding with polyanionic targets, such as heparin.[21,22] Reports have demonstrated the possibility for heparin recovery by crosslinking chitosan into microbeads or immobilizing chitosan on microbead scaffolds.[23,24] Though improvements in heparin-recovery performance have been reported, chitosan is difficult to recycle in multiple capture cycles and its heparin-recovery capacity remains low.

Cellulose nanocrystals (CNC) are anticipated to make a major impact to substitute synthetic materials.[25–27] CNC is produced by the hydrolysis of cellulose, the most abundant polysaccharide found in all green plants.[28] Aside from the renewability and sustainability, CNC is mechanically and chemically robust owing to the highly crystalline domains while the dense hydroxyl groups make diverse surface modifications feasible on CNC.[25,29] Therefore, CNC has been widely applied in material science and nanotechnology, and is gaining increasing interest in biological applications, such as biosensing and medical scaffolds.[25,27,30,31] In this work, we further extended its application scope by employing CNC for fast, efficient and selective heparin recovery. Poly(*N,N*-dimethylaminoethyl methacrylate) (p(DMAEMA)) was firstly grafted from CNC surface *via* a surface-initiated atom-transfer radical polymerization (SI-ATRP). The amine groups in the obtained CNC hybrid were quaternized subsequently, yielding a positively charged CNC with a brush-like structure, termed as pCNC. Nuclear magnetic resonance (NMR) spectroscopy, Fourier-transform infrared (FTIR) spectroscopy, dynamic light scattering (DLS) measurements, atomic force microscopy (AFM) and transmission electron microscopy (TEM) confirmed the successful production and the cationic nature. The effective binding between pCNC and heparin was demonstrated with methylene blue (MB) binding assay and quartz crystal microbalance with dissipation monitoring (QCM-D) tests. Importantly, we found that the selective heparin-capture over serum albumin (SA) protein can be realized *via* adjusting the salt concentration or pH. Finally, the recyclability of pCNC was evaluated and compared with a commercial heparin-recovery resin, Amberlite IRA-900, and the effective heparin dose in the recycled heparin samples was measured. This CNC hybrid exhibits excellent heparin-recovery capacity and selectivity, thus presents a promising alternative to replace the currently used resins.

2. Material and methods

2.1. Chemicals and materials

α-bromoisobutyryl bromide (BriBBr), 4-dimethylaminopyridine (DMAP), *N,N*-dimethylaminoethyl methacrylate (DMAEMA), Copper(I) bromide (Cu(I)Br), hexamethyltriethylenetetramine (HMTETA), ethyl α-bromoisobutyryl bromide (EBiB), methyl iodide (MeI), methylene blue (MB), heparin sodium salt from porcine intestinal mucosa (100 KU/503.7 mg) and serum albumin (SA, ~66 kDa) protein were purchased from Sigma-Aldrich and used without further purification. Amberlite® IRA-900 chloride form was obtained from Sigma-Aldrich.

2.2. Material preparation

2.2.1. CNC preparation

CNC was prepared from ground Whatman 541 ashless filter paper (Whatman GmbH, Dassel, Germany) *via* sulfuric acid hydrolysis technique with added ion-exchange and purification steps.[32] In brief, mechanically disintegrated (kitchen blender) filter paper (10 g) was transferred into a 1 L three-neck flask. Then, sulfuric acid solution (64 wt %, 175 mL) was added, and the hydrolysis procedure was carried out at 45 °C for 45 minutes (min) using mechanical stirring. Afterwards, the reaction was quenched by pouring into Milli-Q water (1.8 L). The crude product was precipitated, collected by centrifugation, and dialyzed against Milli-Q water (membrane: SpectraPor® 7, MWCO 3.5 kDa) to a conductivity of less than 5 mS. After the dialysis, the CNC dispersion was filtered through a Whatman 541 ashless filter paper and the pH was adjusted to 7 with sodium hydroxide solution (0.1 M), followed by another dialysis against Milli-Q water and subsequent freeze-drying. The obtained solid was washed with Soxleth extraction for 48 h using ethanol. Finally, the product was freeze-dried and eventually redispersed just before the relevant experiments. The surface charge was determined to be 0.6 e nm^{-2} by conductometric titration, and the dimension was derived from AFM images.

2.2.2. pCNC preparation

The preparation of pCNC followed a reported procedure which included three main steps: CNC surface deposition with the initiator BriBBr, SI-ATRP of DMAEMA, and the final quaternization of p(DMAEMA).[33]

BriBBr deposition on CNC. BriBBr was firstly deposited on CNC *via* a chemical vapor deposition (CVD).[34] Briefly, CNC (1 g) in a 30 mL glass vial was immersed in a bigger glass container that contained BriBBr (2 mL, 16.18 mmol). The big glass container was sealed and covered from light, and the reaction was carried out overnight. Afterwards, the crude was purified through consecutive washing (dimethylformamide (DMF), acetone, ethanol, and hexane) and centrifugation cycles and finally freeze-dried from 1,4-dioxane. Next, the pretreated CNC (500 mg) was dispersed in dry DMF (50 mL) and kept under N_2 atmosphere. Pyridine (1.5 mL) and DMAP (32 mg, 0.26 mmol) were added, and the solution was cooled down to 0 °C. Then, BriBBr (1.5 mL, 12.1 mmol) was added dropwise, and the reaction was carried out for 30 min. Afterwards, the reaction was evaluated to room temperature and continued for another 48 h. The product (CNC-iBBr) was purified through consecutive washing (DMF, acetone, ethanol, and hexane) and centrifugation cycles, and finally it was extracted using Soxhlet with dichloromethane and dried. The CNC-iBBr was characterized with FTIR and ^{1}H NMR.

SI-ATRP of DMAEMA. CNC-iBBr (200 mg) was dispersed in dry DMF (6 mL) *via* bath sonication and transferred to a two-necked flask, and DMAEMA (5.83 mL, 17.31 mmol) was added. The flask was sealed with a cap and a septum, the mixture was stirred using a magnetic stirrer and oxygen was removed from the reactor by bubbling N_2 through the mixture. Cu(I)Br (57.6 mg, 0.40 mmol) was then added, and the mixture was purged with N_2 again. A solution of the sacrificial initiator EBiB (27.4 μL, 0.19 mmol) and HMTETA (203 μL, 0.75 mmol) in dry DMF (4 mL) was simultaneously purged with N_2. Then, the CNC-iBBr mixture was heated to 70 °C in a water bath and the EBiB-HMTETA solution was added dropwise using a double-tipped needle. After 2 h, the reaction was stopped and cooled down to room temperature. The product was purified through consecutive washing (methanol, 20 mL) and centrifugation cycles, and the supernatant containing free polymers was collected. The washed precipitate was redispersed in dry DMF (20 mL) and further purified by several redispersion and centrifugation cycles in different organic solvents (3 × DMF and 3 × 1,4-dioxane). The final p(DMAEMA) grafted CNC product was collected and freeze-dried from 1,4-dioxane, and was characterized with FTIR and ^{1}H NMR. The collected supernatant containing the p(DMAEMA) homopolymer was used to follow the kinetics of the polymerization with gel permeation chromatography (GPC).

Quaternization of p(DMAEMA) grafted CNC. p(DMAEMA) grafted CNC (200 mg) was dispersed in Milli-Q water (20 mL), and MeI (2 mL) was then added. The reaction was allowed to carry out for 7 days. After the reaction, the excess MeI was evaporated from the solution and the crude product was purified through consecutive washing (water) and centrifugation cycles, and finally freeze-dried. The final quaternized product, pCNC, was characterized with FTIR, AFM and TEM. The quaternization of p(DMAEMA) polymer followed the same procedure.

2.3. Material characterization

Fourier-transform infrared spectroscopy (FTIR). FTIR were inspected by Spectrum Two FTIR Spectrometer (PerkinElmer, Inc., Germany) to study the chemical structure of the materials. Thirty-two scans were conducted and spectra in an absorbance mode between 4000 cm^{-1} and 400 cm^{-1} wavenumber range at 1 cm^{-1} resolution were collected.

Dynamic light scattering (DLS). Zeta potential was recorded using a Zetasizer Nano-ZS90 instrument (Malvern, UK). It was determined with a dip cell probe and calculated from the electrophoretic mobility data using a Smoluchowski model. A volume of 0.5 mL was collected for all measurements with a concentration of 0.5 mg mL^{-1}. The size determination was carried out on the same device with a 4 mW He − Ne ion laser at the wavelength of 633 nm and an Avalanche photodiode detector at an angle of 173°. Zetasizer software (Malvern Instruments) was used to attain the data. Cumulant analysis was used to obtain the intensity mean value of the complex size, that is, the hydrodynamic diameter. Experiments were carried out at 25 °C. pCNC was dispersed in 300 μL phosphate buffer (PB, 10 mM, pH 7.4) with a concentration of 0.1 mg mL^{-1} and 3 μL heparin in the same solution was added, yielding the desired mass ratio. Three measurements for each sample were conducted to evaluate the reproducibility of the measurement.

Transmission electron microscopy (TEM). CNC or pCNC dispersion was deposited on carbon films in copper square mesh grids and dried under ambient conditions. Negative staining of the samples was made with 3 wt% uranyl acetate. TEM images were acquired in bright-field mode on a FEI Tecnai 12 (USA) operating at 120 kV.

Atomic force microscopy (AFM). CNC or pCNC was spin-coated on a silicon wafer by using a WS-650SX-6NPP/LITE spin coater (Laurell Technologies Corporation, North Wales, PA). Before spin-coating, the silicon wafers were cleansed for 15 min in a UV-ozonator (Bioforce Nanosciences Inc., CA). Spin-coating was carried out at 4000 rpm with an acceleration of 4000 rpm/s for approximately 90 s. AFM imaging was carried out with a MultiMode 8 Scanning Probe Atomic Force Microscope from Bruker AXS inc. (Madison, WI). Images were taken using an E-scanner in tapping mode with NSC15/AIBS silicon cantilevers by Ultrasharp μmasch (Tallinn, Estonia). According to the manufacturer, the radius of curvature of the tips was less than 10 nm with a typical cantilever resonance frequency of 325 kHz. AFM images were analyzed using Nanoscope Analysis 1.20 software.

Methylene blue (MB) binding assay. The time-dependence of the heparin-capture ability was evaluated by adding pCNC or Amberlite IRA-900 to heparin in PB, yielding a final solution of 5 mL containing 0.5 mg mL^{-1} heparin and 10 mg mL^{-1} pCNC or Amberlite IRA-900. After every 10 min, 100 μL solution was taken and precipitated by centrifugation. The heparin concentration in the supernatant was determined with the help of MB.[17] A calibration curve was plotted using the absorbance intensity ratio A (664 nm)/A (568 nm) of MB (0.013 mg mL^{-1}) against the heparin concentration between 0 and 20 μg mL^{-1} (Fig. S1). The absorption spectra of the samples were measured with a BioTek Cytation 3-microplate reader in a 96-well plate at room temperature (400–750 nm). Measurements were performed using triplicate samples.

The influence of pH (5.0, 7.4 and 9.0) on the heparin-binding ability was measured following a similar procedure. Different concentrations of the binders were added to the heparin solution (0.5 mg mL^{-1}) in 10 mM phosphate buffer with a corresponding pH, yielding desired mass ratios. After mixing and precipitation, the heparin concentration in the supernatant was determined with the help of MB (0.013 mg mL^{-1}) by measuring the absorbance intensity ratio A (664 nm)/A (568 nm). Measurements were performed using triplicate samples.

Quartz crystal microbalance with dissipation monitoring (QCM-D). Interactions between surface immobilized pCNC or CNC and heparin or SA were investigated by using gold-coated sensors and a QCM-D unit (E4 instrument, Q-Sense AB, Sweden). To start, the areal mass of the spin-coated pCNC or CNC (3 mg mL^{-1}) thin film was determined as described by Peresin *et al.* by determining the frequency response in air (normal atmospheric conditions) before and after pCNC or CNC film deposition on the QCM-D sensor crystal.[35] The collected frequency data were stitched together using Q-Tools Software, and the areal mass was calculated according to the Sauerbrey equation:

$$\Delta m = (-C \cdot \Delta f)/n$$

where $\Delta f = f - f_0$ is the resonance frequency, n is the measurement overtone number ($n = 1, 3, 5, 7, \ldots$), and C is the sensitivity constant of the sensor.[36] Each sample was first dried in an oven at 80 °C for 15 min prior to the mass change determination. Before the heparin or SA adsorption measurements, the pCNC or CNC thin films were allowed to stabilize in buffer. Then, the heparin or SA adsorption experiments were carried out, followed by Milli-Q washing. After that, the sensors were dried in an oven at 80 °C for 15 min and the areal mass of tested sensors were calculated by determining the frequency response in air (normal atmospheric conditions). All target molecules were dissolved in PB without or with 150 mM NaCl to yield 0.1 mg mL^{-1} concentration. All solutions were filtered by using 0.45 μm filters prior to tests. Experiments were performed at a constant flow rate of 20 μL min^{-1}, and the temperature was maintained at 23 °C. Voigt protocol (Q-Tools software, version 2.1, Q-Sense, Västra Frölunda, Sweden) was used to estimate the adsorbed mass of polymer layer on the pCNC or CNC surface.

Heparin and SA capture by pCNC. To determine the effect of salt concentration (PB, NaCl: 0.15 M, 0.5 M, 1 M, 2 M, 4 M, and brine) and pH (10 mM phosphate buffer, NaCl: 150 mM, pH: 5, 6, 8, 9, and 10) on the heparin or SA capture ability of pCNC, 10 mg mL^{-1} pCNC was mixed with 0.5 mg mL^{-1} heparin or SA in 500 μL corresponding solution, and the solution was incubated for 10 min at room temperature. Afterwards, the mixture was precipitated *via* centrifugation and 200 μL supernatant was taken and dialyzed against Milli-Q water for 48 h (Slide-A Lyzer® MINI Dialysis Units, MWCO 3.5 kDa). After freeze-drying, the sample was redissolved in PB and the concentration was determined. Heparin concentration was measured by using the calibration curve with the help of MB (Fig. S1). To determine the SA concentration, a calibration curve was plotted using the absorption at 280 nm against SA concentration (Fig. S2). Measurements were performed using triplicate samples.

pCNC recyclability. To determine the recyclability of pCNC, 10 mg mL^{-1} pCNC was mixed with 0.5 mg mL^{-1} heparin in 1 mL phosphate-buffered saline (PBS: PB, 150 mM NaCl) and incubated on a shaker at room temperature for 10 min. Then, the precipitate was isolated by centrifugation, and 800 μL supernatant was discarded. The remaining precipitate was purified with consecutive washing (3 × PBS, 800 μL) and centrifugation cycles to remove the unbound heparin. Afterwards, 800 μL brine was added to the pCNC-heparin complex to release heparin, and the solution was incubated on a shaker at 50 °C for 90 min. After the incubation, the solution was centrifugated, and 800 μL supernatant was collected and dialyzed against Milli-Q water for 48 h to remove salt (Slide-A Lyzer® MINI Dialysis Units, MWCO 3.5 kDa). Finally, the dialyzed sample was freeze-dried and redissolved in 800 μL PB for concentration determination using the method given above. The remaining precipitate was purified with consecutive washing (3 × NaCl (4 M in PB), 3 × PB and 3 × PBS) and centrifugation cycles. Finally, the precipitate was redispersed in PBS and heparin was added, yielding a 1 mL solution with 0.5 mg mL^{-1} heparin. The heparin recovery procedure was repeated to determine the recyclability of pCNC. The heparin recovery performance of Amberlite IRA-900 was followed by using the same procedure. The determination of the SA amount in the recovered heparin sample in the first round followed the same procedure by mixing heparin and SA (each 0.5 mg/mL) with 10 mg mL^{-1} pCNC in PBS. Measurements were performed using triplicate samples.

Anti-Xa assay. The active heparin dosage in the recovered heparin samples was evaluated using a commercial two-stage kit, BiophenTM Anti-Xa (221005). After concentration measurement, the recovered heparin samples were diluted to 0.2 μg mL^{-1} and the kit reagents were

utilized according to the manufacturer's instructions to determine effective heparin dosage. To run the calorimetric assay, 40 μL of the sample solution was added to a 96-well microplate followed by the addition of 40 μL of antithrombin and incubation for 2 min. Then, 40 μL of factor Xa was added and incubated for another 2 min. Afterward, 40 μL of the factor Xa- specific chromogenic substrate was added to the solution and let react for 2 min. Finally, the reaction was quenched by introducing 80 μL of 2% citric acid. The absorbance at 405 nm was recorded immediately using a BioTek Cytation 3-microplate reader. The anticoagulant activity is inversely proportional to the measured absorption intensity, and the effective heparin dosage was determined using a calibration curve constructed according to the manufacturer's instructions (Fig. S3). The effective heparin rate was calculated using the following equation:

$$3.\ wt\% = [(c_t/0.2)/c_0] \times 100$$

where c_t is the measured effective dose in 0.2 μg mL^{-1} heparin and c_0 is the original value from the manufacturer which is 0.2 IU μg^{-1}. Measurements were performed using triplicate samples.

4. Results and discussion

4.1. Material preparation and characterization

The preparation of pCNC followed a reported procedure,[33] and it is illustrated in Fig. 1a. To yield a high grafting degree, the deposition of the initiator, BriBBr, on CNC was accomplished *via* an initial CVD step and an additional coupling in solution.[34] Successful reaction was verified with FTIR (Fig. 1b) and ^{1}H NMR (Fig. S4). Comparing to the pristine CNC (Fig. 1b), a new stretching band at 1743 cm^{-1} corresponding to the carbonyl groups from iBBr emerged while the hydroxyl groups at 3340 cm^{-1} originating from the sugar units in CNC remained unchanged.[34] Subsequent SI-ATRP of DMAEMA resulted in the p(DMAEMA) polymer chains on the crystal surface, as proved by FTIR (Fig. 1b) and ^{1}H NMR (Fig. S5). The addition of the sacrificial initiator, EBiB, has been reported to benefit the chain propagation on CNC while produce free homopolymers in solution that are largely identical to those on CNC.[34,37] Therefore, the chain length and the polydispersity of the p(DMAEMA) on CNC were deducted by analyzing free polymers in the solution with GPC. The GPC result showed a averaged number molecular weight (M_n) of 61 000 g mol^{-1} with a molar-mass dispersity of 1.23, suggesting a relatively uniform polymer length on CNC (Fig. S6).[33] After quaternization, the signals between 2700 and 2800 cm^{-1} corresponding to $-N(CH_3)_2$ groups disappeared while bands at 1142 cm^{-1} (–C–N <), 1475 cm^{-1} ($-CH_2-$), 1724 cm^{-1} (>C = O) and 2950 cm^{-1} ($-CH_2-$, $-CH_3$) that were associated with p(DMAEMA) polymer remained (Fig. 1b and Fig. S7), indicating the successful production of pCNC.

We compared the morphologies of the obtained pCNC and the pristine CNC by using AFM and TEM (Fig. 2c-g and Fig. S8). The images of unmodified CNC showed aggregates of rod-shaped objects with a smooth surface (Fig. 1c and Fig. S8). After cationization, pCNC was homogeneously dispersed, and clear boundaries can be distinguished between pCNC particles (Fig. 1d,e). Besides, the shape was shifted to a round bar-like structure with a rough surface. Fig. 1f revealed that pCNC had a relatively shorter crystal length with a narrower size distribution comparing to CNC. Height profiles taken perpendicular to the crystals on AFM images showed clear size increases in height and width, which, together with the TEM images, indicate the existence of the polymer layer.[33]

We also determined the surface zeta potential (ξ) with

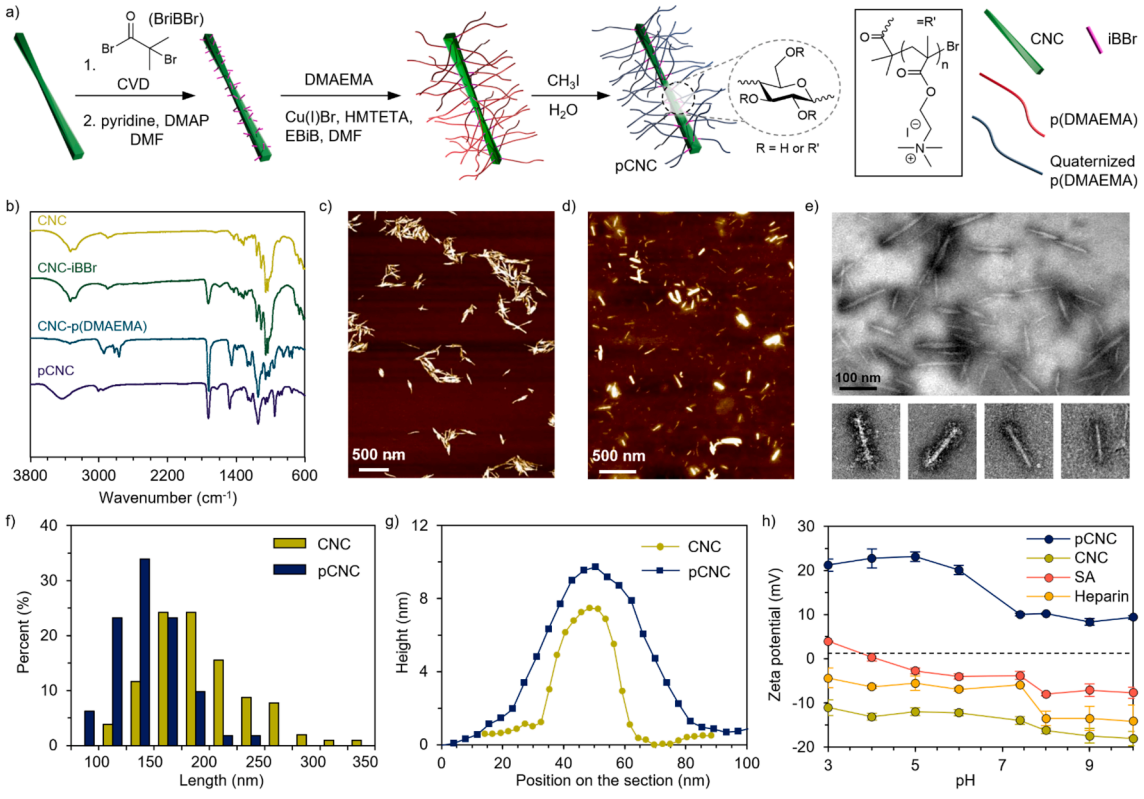

Fig. 1. (a) Schematic illustration of the pCNC preparation procedure. (b) FTIR spectra of pristine CNC, iBBr deposited CNC, p(DMAEMA) grafted CNC, and pCNC. (c) AFM image of CNC. (d) AFM image of pCNC. (e) Representative TEM images of pCNC. (f) Length distribution histogram estimated from the AFM images of CNC and pCNC (total number: 103 for CNC and 112 for pCNC). (g) Representative height profiles of CNC and pCNC. (h) Zeta potential of CNC, pCNC, SA and heparin measured at different pH values. Measurements were performed using triplicate samples, and the averaged results with standard deviation are presented.

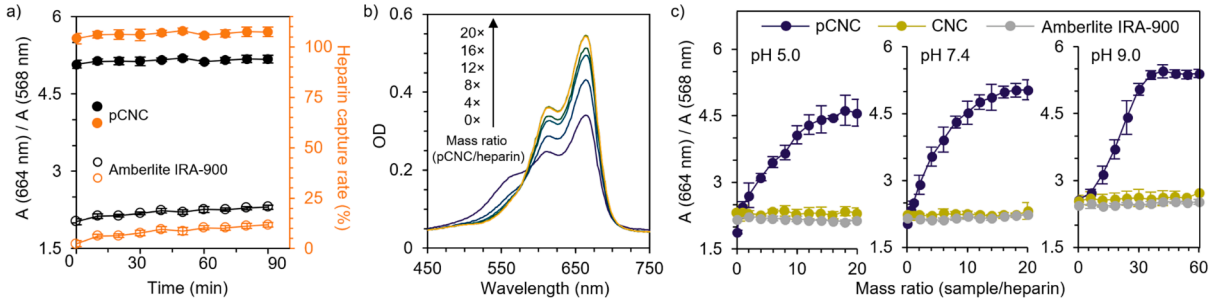

Fig. 2. (a) Time-dependence of the heparin-capture performance of pCNC and Amberlite IRA-900 in PB, measured by the MB binding assay and reported as the A (664 nm)/A (568 nm) ratio as well as the calculated heparin-capture rate (wt%). (b) Representative UV–vis spectra of the MB binding assay of pCNC performed in PB. (c) MB binding assay results at different pH (5.0, 7.4 and 9.0) in 10 mM phosphate buffer, measured by the A (664 nm)/A (568 nm) ratio. All measurements were performed using triplicate samples, and the averaged results with standard deviation are presented.

electrophoretic light scattering in response to pH change. As shown in Fig. 1h, the zeta potential of all tested samples decreased as the pH was elevated. Owing to the surface sulfonate anions, CNC was negatively charged (ξ < -10 mV) in the whole pH range.[33] After the surface modification, the anionic nature was shielded by the polymer layer, and CNC with a cationic surface (ξ greater than 10 mV) was obtained in the tested pH range. While SA displayed a typical surface charge transition at approximately pH 4,[38] heparin stayed anionic in the whole pH range because of the dense carboxylic and sulfonate groups.[2,24]

4.2. Heparin binding

After verifying the successful preparation of pCNC, we compared the heparin-binding ability of pCNC, CNC and a commercial heparin-recovery resin, Amberlite IRA-900, in PB using a MB binding assay.[39–41] Unlike the previously reported systems that took half to one hour to reach a binding equilibration,[17,24] pCNC instantaneously captured all heparin in solution upon mixing the two polyelectrolytes, as shown in Fig. 2a (solid dot). On the contrary, heparin-binding to Amberlite IRA-900 gradually increased and only ~ 12 wt% heparin was captured after 90 min (hollow circle). When the resin concentration was increased 10 times (100 mg mL^{-1}, mass ratio: 200), only ~ 4 wt% heparin was captured by the resin when heparin was added, and this value gradually reached ~ 75 wt% after 90 min incubation (Fig. S9).

Later, the heparin-binding ability was evaluated at various pH (5.0, 7.4 and 9.0) in 10 mM phosphate buffer (Fig. 2b,c). It is worth noting that the complexation between absorbents and heparin was immediately followed by the precipitation procedure without an incubation step on a shaker. We found that the quaternized p(DMAEMA) polymer exhibited an excellent heparin-binding performance which reached saturation points at mass ratios of ~ 2 in all conditions (Fig. S10), exhibiting a similar capacity as the clinical heparin antidote, protamine sulfate.[39–41] pCNC also showed obvious binding to heparin (Fig. 2b,c), and the best performance was observed at pH 7.4 with a saturation point at a mass ratio of ~ 16 while those at pH 5.0 and 9.0 were ~ 18 and ~ 36, respectively, a trend that was also observed with other heparin absorbents.[17,24] The decreased binding efficiency comparing to quaternized p(DMAEMA) polymer originated from CNC crystals which lowered the charge-to-mass ratio but played a vital role in the heparin-recovery process, as demonstrated in Section 3.3. On the other hand, no binding between heparin and CNC was observed, which was expected as both chemicals were negatively charged (Fig. 1h). The binding between heparin and Amberlite IRA-900 was not detectable in the tested conditions (Fig. 2c), and a further increase to 1000 showed slight enhancement in the binding performance (Fig. S11). Combining the results, we found that the binding between Amberlite IRA-900 and heparin in PB was inefficient and significantly affected by the incubation time. On the contrary, the polycation-grafted CNC exhibited high heparin-capture ability and performance over time. We attribute the excellent heparin-binding performance of pCNC to the multivalent electrostatic interaction between the flexible cationic p(DMAEMA) polymer brush and the highly negatively charged heparin.[41,42] On the contrary, the ammonium cations on Amberlite IRA-900, as well as the microbeads,[23,24] are relatively sparse and constrained, which leads to restricted molecular movement and the subsequent weak electrostatic interaction. Besides, the screening effect of ions in the buffer can further weaken the interaction between the cationic beads and heparin. The much smaller size of pCNC (100–300 nm, Fig. 1f) compared to Amberlite IRA-900 (300–1190 μm) yields a highly increased specific surface area, which can also contribute to the efficient interaction with heparin.

The capture ability was also evaluated with QCM-D by measuring changes in resonance frequency shifts (Δf) and energy dissipation (ΔD) as a function of time under constant flows. CNC or pCNC was firstly deposited on a gold-coated sensor *via* spin-coating, which was followed by flushing with a constant heparin or SA solution flow. The shifts in the resonance frequency and energy dissipation were recorded (Fig. 3a-d). Dramatic frequency changes were observed when pCNC was flushed with heparin in PB without (Fig. 3a) or with (Fig. 3b) salt (150 mM NaCl), demonstrating the excellent heparin-capture ability of pCNC even under physiologically relevant conditions. A similar trend was also observed with pCNC capturing SA in PBS (Fig. 3c). However, the frequency curves for CNC coated sensors flushed with heparin stayed almost unchanged (Fig. 3d), implying no binding between the two components. Based on the frequency/mass relation (Sauerbrey equation), we calculated the initial weights of CNC or pCNC deposited on the sensors and the absorbed target mass after the tests, and the normalized weights are compared and presented in Fig. 3e. It showed that adding NaCl (PBS) had a minor effect on the binding between pCNC and heparin (88 ng/100 ng pCNC in PB *vs* 81 ng/100 ng pCNC in PBS). In PBS, the bound mass of SA was 44 ng/100 ng pCNC while CNC showed negligible binding to heparin (8.8 ng/100 ng CNC in PB) even in the absence of salt, which is well in line with the MB binding result.

Energy dissipation (ΔD) results confirmed the binding performance of all samples (Fig. 3a-d, insets). After the initial rinsing with buffer, a subsequent heparin flow had a negative influence on the energy dissipation of pCNC in both conditions (Fig. 3a,b, insets), which can be explained by the increased surface rigidity caused by the polyelectrolyte complexation.[39] On the other hand, heparin had no detectable influence on CNC (Fig. 3d, insets) while a positive shift was observed with pCNC flushed with SA (Fig. 3c, insets), implying the increase in viscoelasticity that was caused by the bound SA.

Comparing to the heparin-capture capacity deduced from MB binding assay (mass ratio of 16 at saturation point at pH 7.4, corresponding to a capture capacity of ~ 62 mg g^{-1}), we found that the capacity was greatly enhanced when pCNC was deposited on sensors (880 mg g^{-1}). The clear difference was reasoned to be the different binding models in the two conditions, as illustrated in Fig. 3f. In solution (MB binding assay), a small amount of heparin can interconnect and precipitate well

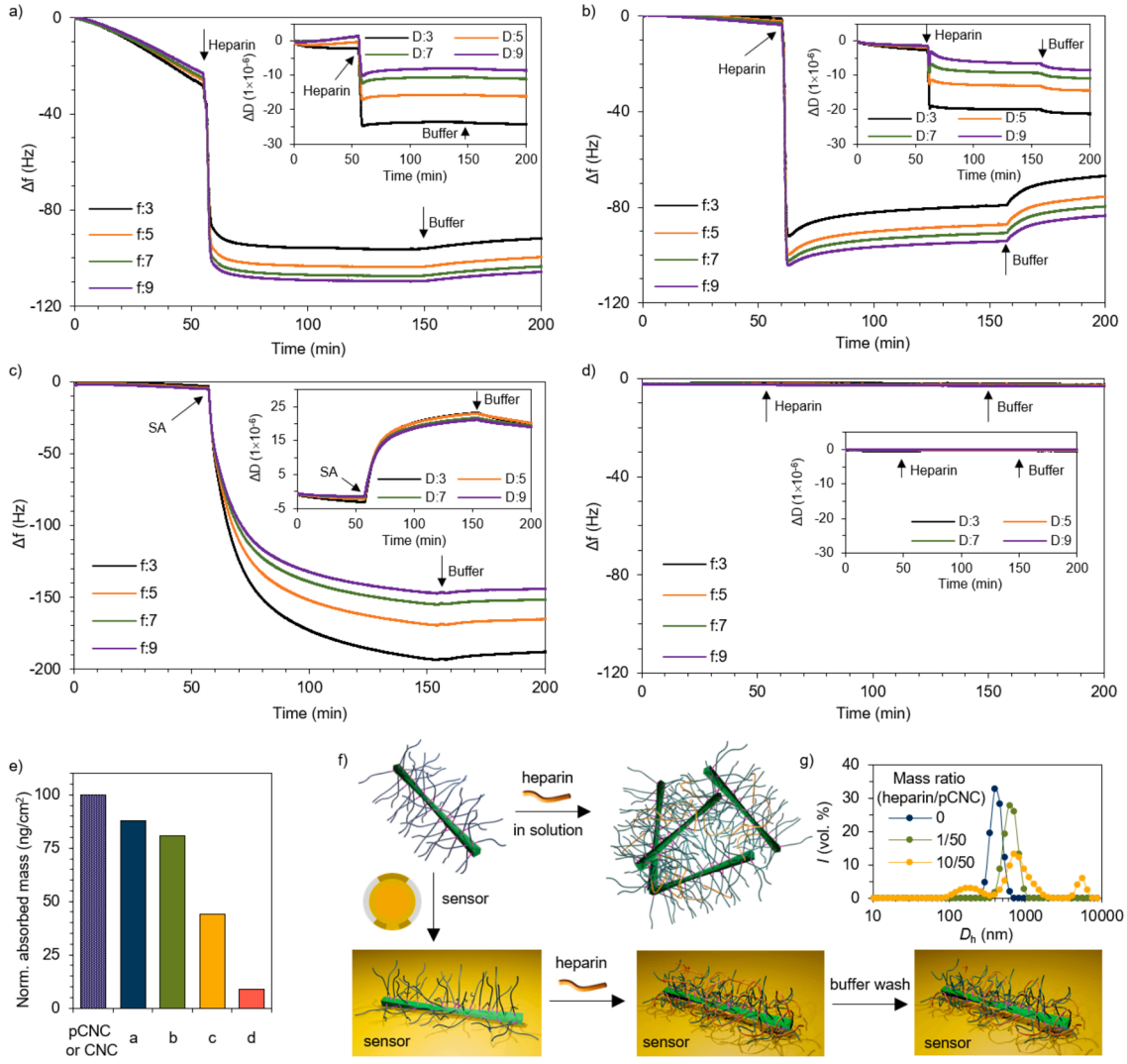

Fig. 3. Frequency shifts (Δf) and energy dissipation (ΔD) graphs (insets) from QCM-D measurements on the evaluation of (a) pCNC capturing heparin in PB, (b) pCNC capturing heparin in PBS, (c) pCNC capturing SA in PBS, and (d) CNC capturing heparin in PB. (e) The normalized weights of CNC or pCNC deposited on the sensors and the captured target mass derived from frequency shifts in graph a-d. (f) The proposed pCNC binding heparin models in solution and on the sensor. (g) The presentative pCNC solution titrated with heparin in different mass ratios in PB measured by DLS.

dispersed pCNC nanoparticles, forming insoluble complexes and preventing pCNC from further capturing heparin. This proposed mechanism was supported by the DLS measurement (Fig. 3g). When pCNC was deposited on a sensor, though the mobility was constrained and some polycations were inaccessible to heparin, no complex precipitation was expected, and a large amount of free polymers on pCNC were capable of

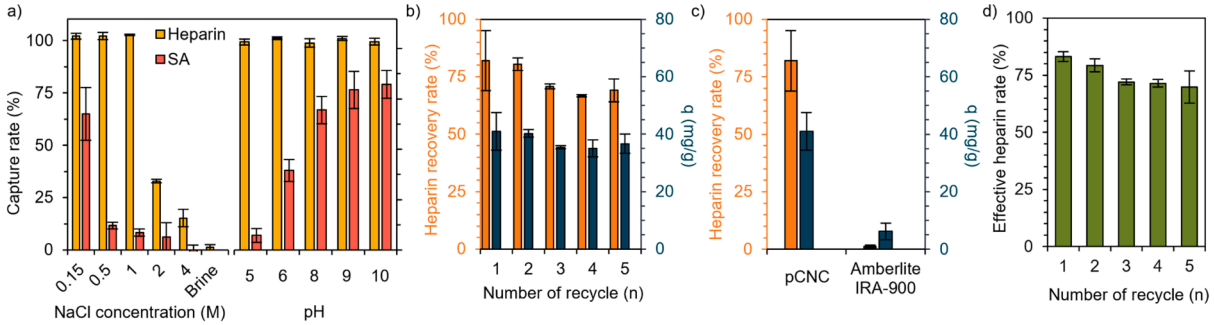

Fig. 4. (a) Evaluation on the effect of salt concentration (left, 10 mM PB, pH 7.4) and pH (right, 10 mM phosphate buffer, 150 mM NaCl) on the capture capacity of heparin or SA by pCNC. (b) Study on the recyclability of pCNC in heparin-recovery in PBS. (c) Comparison between pCNC and Amberlite IRA-900 on the heparin-recovery ability in the first recovery round in PBS. (d) Recovery rate of the effective heparin dose measured *via* anti-Xa assay. All measurements were performed using triplicate samples, and the averaged results with standard deviation are presented.

capturing heparin, leading to a highly boosted heparin-capture ability. Therefore, it is reasonable to anticipate that further improvement in heparin-recovery can be achieved by immobilizing pCNC on a scaffold.

4.3. Selective heparin capture and pCNC recyclability

SA was utilized to evaluate the selective binding to pCNC because proteins are the major impurities in crude heparin products.[10] We tested the capture capacity of pCNC towards heparin or SA respectively in various salt concentrations or pH. It was found that selective heparin-capture over SA can be realized *via* adjusting salt concentration or pH, as shown in Fig. 4a. 65 wt% of SA was captured by pCNC in PBS (150 mM NaCl), and the captured amount was significantly affected by salt: increasing NaCl concentration to 0.5 M led to only 10 wt% binding (Fig. 4a, left), a similar phenomenon that was observed with the multi-porous quaternized chitosan/polystyrene microbeads.[24] The binding between SA and pCNC was also remarkably influenced by pH: the capture rate of 82 wt% at pH 10 was lowered to 7 wt% at pH 5 (Fig. 4a, right). This can be explained by the significant change in the surface charge of SA induced by pH (Fig. 1h). On the other hand, the capture rate of heparin remained at 100 wt% even in the buffer containing 1 M NaCl (Fig. 4a, left). This observation can be attributed to the multivalency effect induced by the cationic polyelectrolyte brush.[41–45] Further increase in salt concentration resulted in the decrease in heparin binding and almost no binding was observed in brine. Besides, quantitative heparin-capture was observed in the tested pH range (Fig. 4a, right). Based on these results, we propose an optimal condition for an efficient and selective heparin-recovery: the heparin-capture procedure can be carried out at pH 5 with 1 M NaCl and a subsequent increase in salt concentration can trigger the release of heparin.

The performance of pCNC from an economic perspective was evaluated by recycling pCNC and tracking the change in the heparin-recovery ability in PBS. Fig. 4b showed that 82 wt% heparin was recovered by pCNC in the first recovery round, corresponding to a recovery capacity of ~ 41 mg g^{-1}. This value was 11 times that of the reported multi-porous quaternized chitosan/polystyrene microbeads and 4 times that of the quaternary ammonium functionalized halloysite nanotubes.[17,24] We also evaluated the residual SA in the heparin sample from the first recovery round and found that 43.7 wt% SA was also recovered in PBS, an value that is much smaller than that in the absence of heparin (65 wt%). Based on the result in Fig. 4a, we believe that the selective performance can be further optimized through salt concentration and pH adjustment. After 5 rounds of capture and release cycle, the heparin-recovery capacity was slightly undermined to 36.7 mg g^{-1}, indicating a 69 wt% recovery rate. FTIR result of the recovered product showed identical bands to fresh heparin (Fig. S12). In contrast, the recovery capacity of Amberlite IRA-900 resin was 6.2 mg g^{-1} in the first round, corresponding to a recovery rate of 1.2 wt% in PBS (Fig. 4c). We also evaluated the possibility of using quaternized p(DMAEMA) polymer for heparin recovery. The formation of a white precipitation confirmed the successful binding between the two polyelectrolytes. However, the insoluble complex was dissolved immediately in brine and no separation was realized through centrifugation owing to the similar size of heparin and the quaternized polymer. After the removal of salt, the white precipitation reappeared, and FTIR measurement confirmed the coexistence of the polycations and heparin in the precipitation (Fig. S12), showing an unsuccessful recovery of heparin by using free cationic polymers and highlighting the vital importance of CNC.

We also tested the influence of the capture and release treatment on the active heparin-recovery ability of pCNC. It is recognized that the anticoagulant action is triggered by a particular sequence within heparin chains, which accounts for an active dose of *ca.* 30–40 wt% can inhibit blood-clotting cascade.[46] Therefore, it is essential to guarantee a sufficient active heparin recovery after every recycle round. We analyzed the active heparin dose in the recovered samples after every recycle round with anti-Xa assay (Fig. 4d) and found that more than 80 wt% of the effective heparin was captured in the first recovery cycle and a value of more than 70 wt% was sustained after 5 rounds, demonstrating an excellent heparin-recovery performance.

5. Conclusions

In summary, we employed a biomass-derived material, CNC, to display cationic polyelectrolytes for fast, efficient, and selective heparin-recovery. Successful preparation of the CNC hybrid was confirmed by NMR, FTIR, AFM, TEM and DLS measurements. MB binding assay results unveiled a fast and efficient binding between heparin and pCNC, which exhibited a highly better performance than the commercial heparin-recovery resin, Amberlite IRA-900. QCM-D tests were well in line with these findings and further confirmed the efficient capture in physiological-relevant conditions. Through adjusting salt concentration or pH, selective heparin-capture over a competing binder (SA) can be achieved. An aqueous solution containing 1 M NaCl at pH 5 was found to be optimal for selective heparin-recovery. We also found that the pCNC can be recycled through several capture and release cycles, where most of the active heparin can be recovered at each time. We therefore believe that the reported polymer conjugated CNC presents a promising alternative for a green and efficient heparin production.

Declaration of Competing Interest

The authors declare that they have no known competing financial interests or personal relationships that could have appeared to influence the work reported in this paper.

Acknowledgments

We gratefully thank the Academy of Finland (project nos. 308578, 303804, and 267497), Jane and Aatos Erkko Foundation, Sigrid Jusélius Foundation, and Emil Aaltonen Foundation for financial support. Finn-CERES Academy of Finland Flagship programme (project numbers 318891) is acknowledged for FTIR, AFM and QCM-D. This work was carried out under the Academy of Finland's Centers of Excellence Programme (2014-2019).

Appendix A. Supplementary data

Procedures for NMR and GPC; calibration curves for heparin and SA in PB; a calibration curve for the anti-Xa assay; NMR spectra of the intermediates; GPC result of the p(DMAEMA) polymer; FTIR spectra of the p(DMAEMA) and quaternized p(DMAEMA) polymers; TEM image of CNC; MB binding assay result of Amberlite-IRA900; MB binding assay result of quaternized p(DMAEMA) polymer; FTIR spectra of fresh heparin, heparin recovered by pCNC and quaternized p(DMAEMA) polymer. Supplementary data to this article can be found online at https://doi.org/10.1016/j.cej.2021.129811.

References

[1] B. Casu, A. Naggi, G. Torri, Re-visiting the structure of heparin, Carbohydr. Res. 403 (2015) 60–68, https://doi.org/10.1016/j.carres.2014.06.023.
[2] S.M. Bromfield, E. Wilde, D.K. Smith, Heparin sensing and binding-taking supramolecular chemistry towards clinical applications, Chem. Soc. Rev. 42 (2013) 9184–9195, https://doi.org/10.1039/C3CS60278H.
[3] H. Bussey, J.L. Francis, Heparin overview and issues, Pharmacotherapy. 24 (2004) 103S–107S, https://doi.org/10.1592/phco.24.12.103S.36109.
[4] E.I. Oduah, R.J. Linhardt, S.T. Sharfstein, Heparin: past, present, and future, Pharmaceuticals. 9 (2016) 38, https://doi.org/10.3390/ph9030038.
[5] N.M. Kuderer, A.A. Khorana, G.H. Lyman, C.W. Francis, A meta-analysis and systematic review of the efficacy and safety of anticoagulants as cancer treatment, Cancer. 110 (2007) 1149–1161, https://doi.org/10.1002/cncr.22892.
[6] S. Ma, Z. Mao, Y. Wu, M. Liang, D. Wang, X. Chen, P. Chang, W. Zhang, J. Tang, The anti-cancer properties of heparin and its derivatives: a review and prospect, Cell Adh. Migr. 14 (2020) 118–128, https://doi.org/10.1080/19336918.2020.1767489.

[7] Y. Il Chung, J.C. Kim, Y.H. Kim, G. Tae, S.Y. Lee, K. Kim, I.C. Kwon, The effect of surface functionalization of PLGA nanoparticles by heparin- or chitosan-conjugated Pluronic on tumor targeting, J. Control. Release. 143 (2010) 374–382, https://doi.org/10.1016/j.jconrel.2010.01.017.

[8] B.E. Thacker, D. Xu, R. Lawrence, J.D. Esko, Heparan sulfate 3-O-Sulfation: a rare modification in search of a function, Matrix Biol. 35 (2014) 60–72, https://doi.org/10.1016/j.matbio.2013.12.001.

[9] X. Yang, H. Du, J. Liu, G. Zhai, Advanced nanocarriers based on heparin and its derivatives for cancer management, Biomacromolecules. 16 (2015) 423–436, https://doi.org/10.1021/bm501532e.

[10] J.Y. Van Der Meer, E. Kellenbach, L.J. Van Den Bos, From farm to pharma: an overview of industrial heparin manufacturing methods, Molecules. 22 (2017) 1025, https://doi.org/10.3390/molecules22061025.

[11] N. Volpi, Purification of heparin, dermatan sulfate and chondroitin sulfate from mixtures by sequential precipitation with various organic solvents, J. Chromatogr. B Biomed. Appl. 685 (1996) 27–34, https://doi.org/10.1016/0378-4347(96)00154-5.

[12] I. Capila, R.J. Linhardt, Heparin-protein interactions, Angew. Chemie Int. Ed. 41 (2002) 390–412, https://doi.org/10.1002/1521-3773(20020201)41:3<390::AID-ANIE390>3.0.CO;2-B.

[13] B. Albanyan, E. Laurini, P. Posocco, S. Pricl, D.K. Smith, Self-assembled multivalent (SAMul) polyanion binding—impact of hydrophobic modifications in the micellar core on DNA and heparin binding at the peripheral cationic ligands, Chem. - A Eur. J. 23 (2017) 6391–6397, https://doi.org/10.1002/chem.201700177.

[14] V.M.P. Vieira, V. Liljeström, P. Posocco, E. Laurini, S. Pricl, M.A. Kostiainen, D. K. Smith, Emergence of highly-ordered hierarchical nanoscale aggregates on electrostatic binding of self-assembled multivalent (SAMul) cationic micelles with polyanionic heparin, J. Mater. Chem. B. 5 (2017) 341–347, https://doi.org/10.1039/c6tb02512a.

[15] S. Välimäki, Q. Liu, L. Schoonen, D. Vervoort, N. Nonappa, V. Linko, R.J.M. Nolte, J.C.M. van Hest, M.A. Kostiainen, Engineered protein cages for selective heparin encapsulation, J. Mater. Chem. B. 9 (2021) 1272–1276, https://doi.org/10.1039/d0tb02541k.

[16] H. Eskandarloo, M. Arshadi, A. Abbaspourrad, Magnetic dendritic halloysite nanotube for highly selective recovery of heparin digested from porcine intestinal mucosa, ACS Sustain. Chem. Eng. 6 (2018) 14561–14573, https://doi.org/10.1021/acssuschemeng.8b03188.

[17] H. Eskandarloo, M. Arshadi, M. Enayati, A. Abbaspourrad, Highly efficient recovery of heparin using a green and low-cost quaternary ammonium functionalized halloysite nanotube, ACS Sustain. Chem. Eng. 6 (2018) 15349–15360, https://doi.org/10.1021/acssuschemeng.8b03793.

[18] H. Eskandarloo, M. Arshadi, M. Azizi, M. Enayati, A. Abbaspourrad, High-throughput, green, low-cost, and efficient recovery of heparin from a biological mixture using bio-originated magnetic nanofibers, ACS Sustain. Chem. Eng. 7 (2019) 3895–3908, https://doi.org/10.1021/acssuschemeng.8b04945.

[19] R.C. Thompson, Y. Olsen, R.P. Mitchell, A. Davis, S.J. Rowland, A.W.G. John, D. Mcgonigle, A.E. Russell, Lost at sea: where is all the plastic? Science. 304 (2004) 838, https://doi.org/10.1126/science.1094559.

[20] K.L. Law, R.C. Thompson, Microplastics in the seas, Science. 345 (2014) 144–145, https://doi.org/10.1002/2014EF000240/polymer.

[21] M. Bodnar, J.F. Hartmann, J. Borbely, Preparation and characterization of chitosan-based nanoparticles, Biomacromolecules. 6 (2005) 2521–2527, https://doi.org/10.1021/bm0502258.

[22] K. Kaminski, K. Zazakowny, K. Szczubiałka, M. Nowakowska, pH-sensitive genipin-cross-linked chitosan microspheres for heparin removal, Biomacromolecules. 9 (2008) 3127–3132, https://doi.org/10.1021/bm800724q.

[23] X. Wei, J. Duan, X. Xu, L. Zhang, Highly efficient one-step purification of sulfated polysaccharides via chitosan microspheres adsorbents, ACS Sustain. Chem. Eng. 5 (2017) 3195–3203, https://doi.org/10.1021/acssuschemeng.6b02975.

[24] H. Eskandarloo, M. Godec, M. Arshadi, O.I. Padilla-Zakour, A. Abbaspourrad, Multi-porous quaternized chitosan/polystyrene microbeads for scalable, efficient heparin recovery, Chem. Eng. J. 348 (2018) 399–408, https://doi.org/10.1016/j.cej.2018.04.099.

[25] E. Kontturi, P. Laaksonen, M.B. Linder, A.H. Nonappa, O.J. Gröschel, O.I. Rojas, Advanced materials through assembly of nanocelluloses, Adv. Mater. 30 (2018) 1703779, https://doi.org/10.1002/adma.201703779.

[26] E. Lizundia, D. Pugliac, T.-D. Nguyend, I. Armentano, Cellulose nanocrystal based multifunctional nanohybrids, Prog. Mater. Sci. 112 (2020), 100668, https://doi.org/10.1016/j.pmatsci.2020.100668.

[27] K. Heise, E. Kontturi, Y. Allahverdiyeva, T. Tammelin, M.B. Linder, O. Ikkala, Nanocellulose: recent fundamental advances and emerging biological and biomimicking applications, Adv. Mater. 33 (2020) 2004349, https://doi.org/10.1002/adma.202004349.

[28] D. Klemm, B. Heublein, H. Fink, A. Bohn, Polymer science cellulose: fascinating biopolymer and sustainable raw material, Angew. Chemie Int. Ed. 44 (2005) 3358–3393, https://doi.org/10.1002/anie.200460587.

[29] S. Eyley, W. Thielemans, Surface modification of cellulose nanocrystals, Nanoscale. 6 (2014) 7764–7779, https://doi.org/10.1039/c4nr01756k.

[30] Y. Habibi, L.A. Lucia, O.J. Rojas, Cellulose nanocrystals: chemistry, self-assembly, and applications, Chem. Rev. 110 (2010) 3479–3500, https://doi.org/10.1021/cr900339w.

[31] J.P.F. Lagerwall, C. Schütz, M. Salajkova, J. Noh, J.H. Park, G. Scalia, L. Bergström, Cellulose nanocrystal-based materials: from liquid crystal self-assembly and glass formation to multifunctional thin films, NPG Asia Mater. 6 (2014), e80, https://doi.org/10.1038/am.2013.69.

[32] H. Rosilo, E. Kontturi, J. Seitsonen, E. Kolehmainen, O. Ikkala, Transition to reinforced state by percolating domains of intercalated brush-modified cellulose nanocrystals and poly(butadiene) in cross-linked composites based on thiol–ene click chemistry, Biomacromolecules. 14 (2013) 1547–1554, https://doi.org/10.1021/bm400185z.

[33] H. Rosilo, J.R. McKee, E. Kontturi, T. Koho, V.P. Hytönen, O. Ikkala, M. A. Kostiainen, Cationic polymer brush-modified cellulose nanocrystals for high-affinity virus binding, Nanoscale. 6 (2014) 11871–11881, https://doi.org/10.1039/c4nr03584d.

[34] J. Majoinen, A. Walther, J.R. Mckee, E. Kontturi, V. Aseyev, J.M. Malho, J. Ruokolainen, O. Ikkala, Polyelectrolyte brushes grafted from cellulose nanocrystals using Cu-mediated surface-initiated controlled radical polymerization, Biomacromolecules. 12 (2011) 2997–3006, https://doi.org/10.1021/bm200613y.

[35] M.S. Peresin, K. Kammiovirta, H. Setälä, T. Tammelin, Structural features and water interactions of etherified xylan thin films, J. Polym. Environ. 20 (2012) 895–904, https://doi.org/10.1007/s10924-012-0469-7.

[36] G. Sauerbrey, Verwendung von schwingquarzen zur wägung dünner schichten und zur mikrowägung, Zeitschrift Für Phys. 155 (1959) 206–222, https://doi.org/10.1007/BF01337937.

[37] S.B. Lee, R.R. Koepsel, S.W. Morley, K. Matyjaszewski, Y. Sun, A.J. Russell, Permanent, nonleaching antibacterial surfaces. 1. synthesis by atom transfer radical polymerization, Biomacromolecules. 5 (2004) 877–882, https://doi.org/10.1021/bm034352k.

[38] R. Edelman, Y.G. Assaraf, I. Levitzky, T. Shahar, Y.D. Livney, Hyaluronic acid-serum albumin conjugate-based nanoparticles for targeted cancer therapy, Oncotarget. 8 (2017) 24337–24353. https://doi.org/10.18632/oncotarget.15363.

[39] S. Välimäki, A. Khakalo, A. Ora, L.S. Johansson, O.J. Rojas, M.A. Kostiainen, Effect of PEG-PDMAEMA block copolymer architecture on polyelectrolyte complex formation with heparin, Biomacromolecules. 17 (2016) 2891–2900, https://doi.org/10.1021/acs.biomac.6b00699.

[40] S. Välimäki, N.K. Beyeh, V. Linko, R.H.A. Ras, M.A. Kostiainen, A supramolecular host-guest complex for heparin binding and sensing, Nanoscale. 10 (2018) 14022–14030, https://doi.org/10.1039/c8nr03132k.

[41] Q. Liu, S. Välimäki, A. Shaukat, B. Shen, V. Linko, M.A. Kostiainen, Serum albumin-peptide conjugates for simultaneous heparin binding and detection, ACS Omega. 4 (2019) 21891–21899, https://doi.org/10.1021/acsomega.9b02883.

[42] M.A. Kostiainen, G.R. Szilvay, J. Lehtinen, D.K. Smith, M.B. Linder, A. Urtti, O. Ikkala, Precisely defined protein-polymer conjugates: construction of synthetic DNA binding domains on proteins by using multivalent dendrons, ACS Nano. 1 (2007) 103–113, https://doi.org/10.1021/nn700053y.

[43] M. Mammen, S.K. Choi, G.M. Whitesides, Polyvalent interactions in biological systems: Implications for design and use of multivalent ligands and inhibitors, Angew. Chemie Int. Ed. 37 (1998) 2754–2794, https://doi.org/10.1002/(sici)1521-3773(19981102)37:20<2754::aid-anie2754>3.0.co;2-3.

[44] M.A. Kostiainen, J.G. Hardy, D.K. Smith, High-affinity multivalent DNA binding by using low-molecular-weight dendrons, Angew. Chemie Int. Ed. 44 (2005) 2556–2559, https://doi.org/10.1002/ange.200500066.

[45] G.M. Pavan, A. Danani, S. Pricl, D.K. Smith, Modeling the multivalent recognition between dendritic molecules and DNA: Understanding how ligand “sacrifice” and screening can enhance binding, J. Am. Chem. Soc. 131 (2009) 9686–9694, https://doi.org/10.1021/ja901174k.

[46] H.C. Hemker, S. Béguin, Standard and method independent units for heparin anticoagulant activities, Thromb. Haemost. 70 (1993) 724–728, https://doi.org/10.1021/jacs.8b09143.